NANO LETTERS

pubs.acs.org/NanoLett Letter

Multiphoton Upconversion Enhanced by Deep Subwavelength Near-Field Confinement

Jiahui Xu, Zhaogang Dong, Mohamed Asbahi, Yiming Wu, Hao Wang, Liangliang Liang, Ray Jia Hong Ng, Hailong Liu, Renaud A. L. Vallée, Joel K. W. Yang,* and Xiaogang Liu*

Cite This: *Nano Lett.* 2021, 21, 3044−3051 Read Online

ACCESS | Metrics & More | Article Recommendations | Supporting Information

ABSTRACT: Efficient generation of anti-Stokes emission within nanometric volumes enables the design of ultracompact, miniaturized photonic devices for a host of applications. Many subwavelength crystals, such as metal nanoparticles and two-dimensional layered semiconductors, have been coupled with plasmonic nanostructures for augmented anti-Stokes luminescence through multiple-harmonic generation. However, their upconversion process remains inefficient due to their intrinsic low absorption coefficients. Here, we demonstrate on-chip, site-specific integration of lanthanide-activated nanocrystals within gold nanotrenches of sub-25 nm gaps via bottom-up self-assembly. Coupling of upconversion nanoparticles to subwavelength gap-plasmon modes boosts 3.7-fold spontaneous emission rates and enhances upconversion by a factor of 100 000. Numerical investigations reveal that the gap-mode nanocavity confines incident excitation radiation into nanometric photonic hotspots with extremely high field intensity, accelerating multiphoton upconversion processes. The ability to design lateral gap-plasmon modes for enhanced frequency conversion may hold the potential to develop on-chip, background-free molecular sensors and low-threshold upconversion lasers.

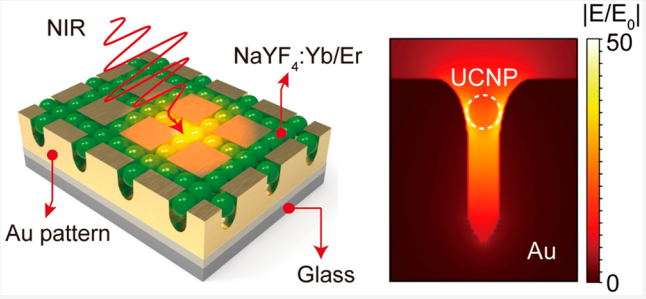

KEYWORDS: *Upconversion, plasmonic nanostructures, self-assembly, nonlinear optical enhancement, deep subwavelength*

Plasmonic nanostructures that can direct and amplify light emission of nanoscale emitters provide suitable platforms for nonlinear optics with ultracompact dimensions.[1−4] Deterministic integration of nonlinear quantum emitters with plasmonic circuits enables the design of chip-scale photonic devices for a host of applications in nanomedicine, photocatalysis, and background-free biosensing.[5−7] For this purpose, controllable and selective positioning of efficient nonlinear emitters onto large-area, predetermined plasmonic circuitry is needed. Many state-of-the-art materials, such as gold and indium tin oxide nanoparticles and two-dimensional MoS_2 nanosheets,[2,8,9] have been exploited as nonlinear active platforms for plasmonic nanodevice coupling. However, anti-Stokes luminescence of given systems is often associated with high-order harmonic generation in which high-power excitation is indispensable due to intrinsically low nonlinear absorption coefficients and thus low conversion efficiencies. Their practical applications are hindered by the need for coherent laser excitation and by the lack of controllability over large assemblies.

Compared with the aforementioned materials, lanthanide-doped upconversion nanoparticles (UCNPs) allow more efficient frequency upconversion due to abundant, physically existing energy states of the lanthanide.[10−16] UCNPs also possess extraordinary optical properties, including excellent photostability, large anti-Stokes shift, low-pumping threshold, and broadly tunable multicolor emission.[17−24] In recent years, the combination of UCNPs and metallic nanostructures have proven effective in enhancing luminescence intensity.[25−35] However, most of the luminescence improvements reported so far for such hybrid nanostructures only range from several to a thousand times in brightness, either due to the insufficient optical density of states within the localized "hotspots" or the inefficient spatial and spectral overlaps between nanoparticles and optical resonators. Besides, the realization of large-scale assembly of UCNPs into well-defined plasmonic circuitry with single-particle resolution has not been achieved, imposing technical constraints on their on-chip integrated photonics.[36]

In principle, metallic nanogaps with ultrasmall mode volume are likely to generate electromagnetic hot spots with extreme near-field enhancement.[37−43] Especially, plasmon enhancement of multiphoton excitation should yield much larger enhancement relative to one-photon excitation due to a

Received: January 19, 2021
Revised: February 28, 2021
Published: March 9, 2021

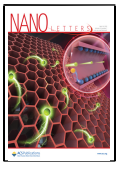

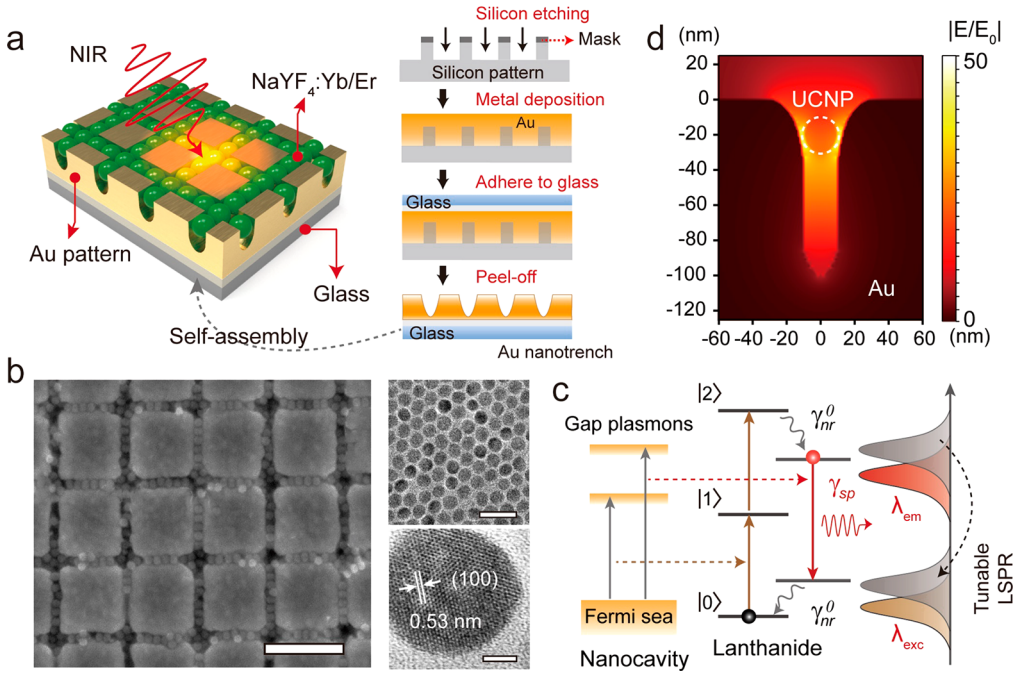

Figure 1. Upconversion emission enhancement through subwavelength confinement of optical fields. (a) Fabrication of gold nanotrenches (sub-25 nm gap) as plasmonic cavities for UCNPs. Briefly, hydrogen silsesquioxane resist was used to fabricate the mask for nanotrenches using electron beam lithography. The silicon substrate was then partially etched using inductively coupled plasma, followed by removing the resist through reactive ion etching. Next, a gold film with a thickness of 150 nm was deposited on the prepatterned silicon substrate by e-beam evaporation. A glass slide adhered to the gold film using optical adhesive glue. After curing, the gold substrate comprising two-dimensional nanotrenches was peeled off. Lastly, UCNPs from the solution self-assembled into nanoscale gaps through capillary force. (b) Left panel: SEM image of UCNPs embedded in square arrays. Scale bar: 200 nm. Right panel: transmission electron microscopy (TEM) image of the as-synthesized $NaYF_4$:Yb/Er nanoparticles (scale bar, 50 nm) and high-resolution TEM image of a single nanoparticle (scale bar, 5 nm). (c) Proposed gap plasmon-coupled upconversion processes. Simplified energy level diagram depicting interactions between gap-plasmon modes and quantum energy levels of UCNPs. Either the accelerated decay or the enhanced upconversion population can be controlled by adjusting the spectral overlap between the localized surface plasmon resonance and the upconversion excitation or emission wavelength. (d) Simulated lateral plasmonic gap-mode with a maximum field enhancement of ~50.

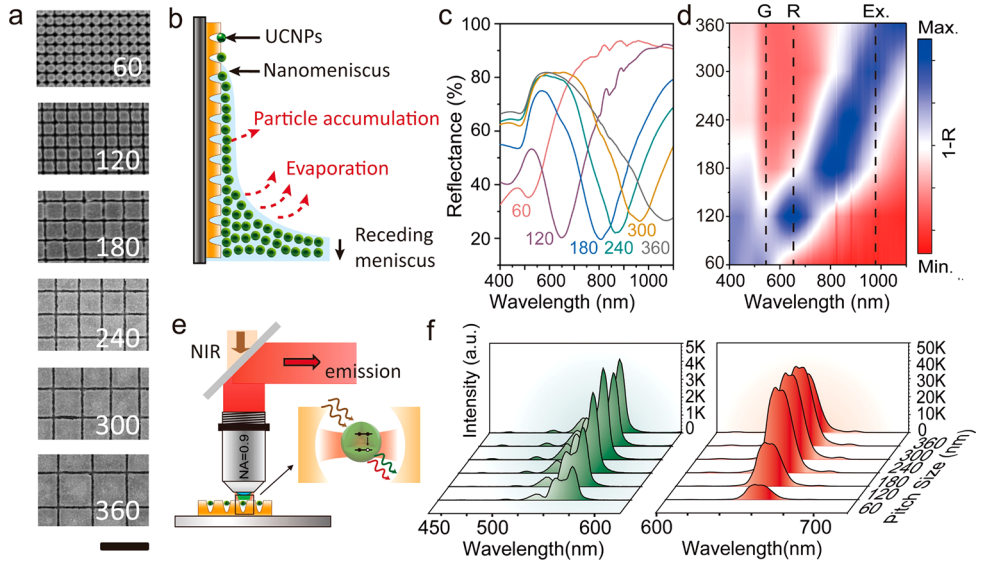

Figure 2. Spectral and optical characteristics of hybrid nanostructures. (a) SEM images of template-stripped gold nanostructures with varying pitch. Numbers indicate pitch sizes in nanometers (scale bar: 500 nm). (b) Schematics of template-assisted dip-coating of UCNPs into gold nanotrenches. Evaporation-induced flow of the solvent lead to particle accumulation. The nanoparticles assemble into the nanotrenches due to the formation of meniscus at the substrate surface. The capillary force induced by the nanomeniscus contact drives the nanoparticles across the substrate until they are physically trapped inside nanotrenches. A more detailed scheme of the nanoparticle assembly is shown in Figure S5. (c) Relative reflectance spectra of UCNP-coupled gold nanotrenches with different pitch sizes (60–360 nm). (d) Color map of the pitch size-dependent reduced reflectance. Dash lines indicate the position of the green (G), red (R) emission and excitation (Ex.) wavelengths. (e) The experimental setup used for the luminescence characterization. (f) Plot of upconversion emission as a function of pitch.

https://dx.doi.org/10.1021/acs.nanolett.1c00232
Nano Lett. 2021, 21, 3044−3051

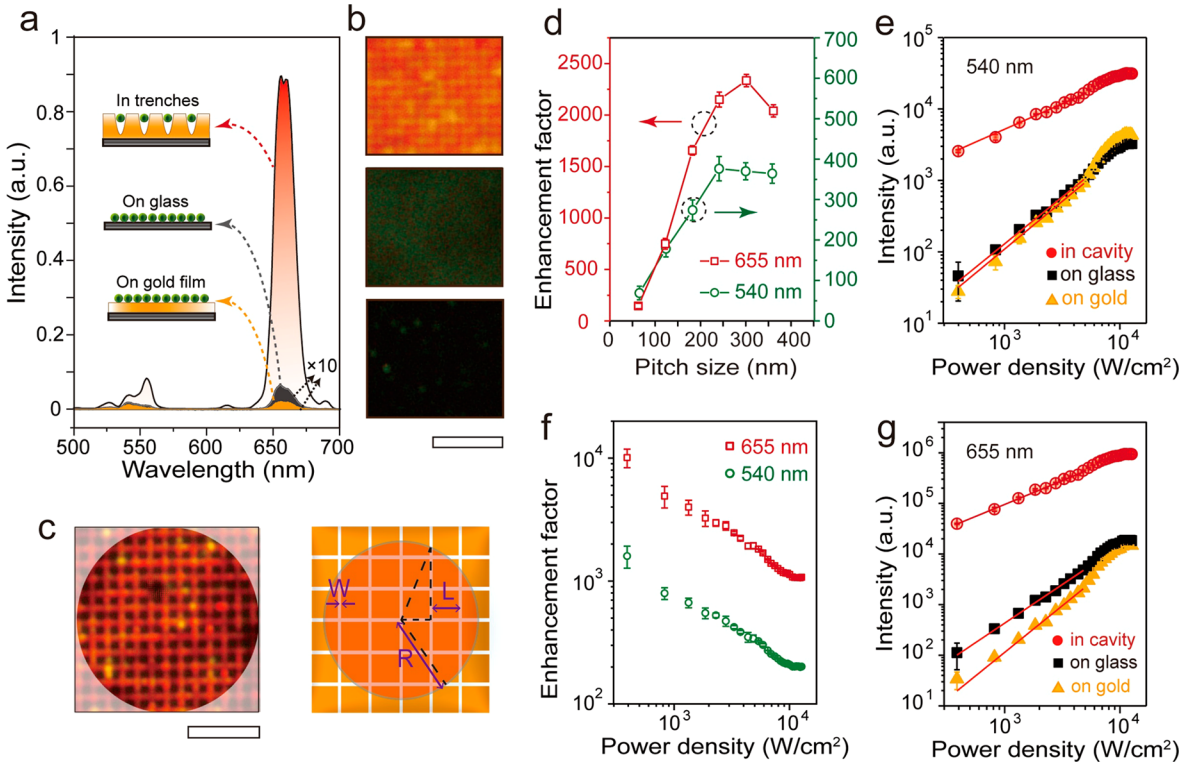

Figure 3. Luminescence enhancement of UCNPs coupled to plasmonic nanotrenches. (a,b) Upconversion luminescence spectra and corresponding fluorescence images of UCNPs assembled within gold nanotrenches with 300 nm pitch (top), on a glass substrate (middle), and on an unpatterned gold film (bottom). Scale bar: 3 μm. (c) Photoluminescence image (left) of UCNPs embedded in a gap-mode nanocavity with a 600 nm pitch size under 980 nm excitation and the area correction scheme (right) used for calculating enhancement factors. Scale bar: 3 μm. (d) Luminescence enhancement factors of nanotrench-coupled UCNPs after effective area correction, compared with samples on a glass slide, as a function of increasing pitch size ranging from 60 to 360 nm. (e,g) Power-dependent measurements of photoluminescence intensity at 540 and 655 nm, performed for the three types of samples. (f) Power-dependent luminescence enhancement (normalized to UCNPs assembled on a glass slide) for nanotrench-coupled UCNPs after effective area correction.

nonlinear dependence of emission on local excitation intensity.[41] Despite these challenges, we reasoned that the combination of template-stripped, smooth metallic nanotrenches with nanoparticle self-assembly may provide a feasible solution.[8,44,45] In contrast to plasmonic systems previously reported, our design not only provides scalable fabrication of deep subwavelength metallic structures with low surface roughness and minimized scattering loss but also offers the possibility for site-specific positioning of UCNPs into nanoscale gaps where the largest field enhancement occurs. Additionally, the fundamental resonance modes of the structures can be systematically tailored to specific wavelengths, promoting excited-state population and radiative transitions.

Here, we experimentally demonstrate an efficient nonlinear platform comprising monolithically integrated UCNPs that self-assemble into gold nanotrenches with sub-25 nm gaps (Figure 1a,b). For an upconversion process to proceed, incident photons are primarily absorbed by sensitizers (such as Yb^{3+} and Nd^{3+}) inside UCNPs and then transferred to adjacent activators (such as Er^{3+} and Tm^{3+}), elevating the electrons in the activators to higher energy states. Subsequently, the electrons emit the accumulated photons and decay back to the ground states. When an UCNP is placed in the vicinity of a plasmonic structure, the strong local electric field induced by the surface plasmon resonance may enhance the photon flux of excitation, leading to improved energy harvesting by sensitizer ions. Concomitantly, the radiative decay rate of the activator would also be increased due to the enhanced local density of states, known as the Purcell effect (Figure 1c). Here, single rows of UCNPs self-assembled into nanotrenches, where the resonant mode under 980 nm irradiation was strongly localized in the gap region with a maximum field enhancement ($|E/E_0|$) of 50 (Figure 1d). Thus, UCNPs are likely to probe a much larger pumping photon flux to excite Yb^{3+} ions from the ground state to the emitting state, leading to dramatically accelerated multiphoton processes and hence enhanced luminescence intensity. In addition, simulation results reveal that the plasmonic hotspot of the cavity is located between metal walls, a situation that further boosts luminescence due to low-level photothermal quenching.

We first validated the feasibility of our strategy to achieve enormously enhanced upconversion luminescence. A template-stripping method based on patterned silicon substrates was used to create plasmonic nanotrenches (Figure 2a and Figure S1).[8] Compared to commonly used metallic nanostructures made by electron-beam lithography (EBL), the template-stripping strategy produces large-area metallic nanopatterns with reduced surface roughness, which decreases plasmon scattering and minimizes intrinsic energy losses (Figures S2 and S3). $NaYF_4$:Yb/Er (18/2 mol %) nanoparticles of ~20 nm in diameter were synthesized for their known efficient upconversion process (Figure 1b and Figure S4).[46,47] Gold nanotrenches with sub-25 nm gaps were fabricated to host a single row of UCNPs. The gap morphology and width were designed to match the particle size, thereby facilitating shape-

https://dx.doi.org/10.1021/acs.nanolett.1c00232
Nano Lett. 2021, 21, 3044−3051

selective nanoparticle immobilization.[8,48] Template-assisted dip-coating was then employed to transfer nanoparticles from the solution to nanotrenches (Figure 2b and Figure S5).[8,45] Scanning electron microscopy (SEM) image indicates that UCNPs are well-positioned in nanoscale gaps, suggesting that deterministic coupling of UCNPs with plasmonic nanostructures is possible by combining top-down lithography and bottom-up self-assembly.

To exploit the maximum emission enhancement of the designed plasmonic platform, a series of gold nanotrenches with different pitch sizes were fabricated while keeping the gap width fixed to ensure the assembly of nanoparticles in well-defined locations (Figure 2a and Figure S6). Relative reflectance spectra of six nanoparticle-containing samples were measured with respect to the unpatterned gold film (Figure 2c and Figure S7). Plasmon resonances, signaled by the dips of the reflectance spectra, monotonically red-shifted with increasing pitch over a broad range of wavelengths, including both emission and excitation regimes. The enhanced absorption of incident energy fluence using metallic nanotrenches was attributed to cavity confinement, which is proportional to reduced reflectance: 1-R (R, reflectance). Reduced reflectance of nanoparticle emitter-containing nanotrenches with different sizes indicates that the absorption enhancement factor increases at a resonance wavelength near 980 nm (Figure 2d).

Luminescence investigation was performed using a custom-built optical microscope (Figure 2e). A continuous-wave 980 nm laser was focused on the samples with a lateral spot diameter of ∼15 μm. The intensity enhancement of the two main emission bands (green at 540 nm and red at 655 nm) of UCNPs was strongly dependent upon the pitch size of the nanotrench (Figure 2f). Notably, the red emission was significantly enhanced when the plasmon resonance mode of the hybrid structure approaches the 980 nm excitation band.

We next measured the luminescence of UCNPs coupled to the gold nanotrench with a 300 nm pitch size and two control samples (UCNPs on a glass substrate and on a gold film) at an excitation power of 6 mW (Figure 3a). The luminescence intensity from UCNPs coupled to gold nanotrenches is substantially larger (>10^2-fold) than that of nanoparticles deposited on control samples (Figure S8). The emission enhancement can be visualized by luminescence imaging. As UCNPs were assembled within nanoscale gaps, we observed a sharp, uniform orange-to-red emission. In contrast, no apparent luminescence was observed for UCNPs deposited on the gold or glass substrate (Figure 3b). Owing to the limited resolution of our imaging system, upconversion emission from nanotrenches with pitch sizes smaller than 300 nm could not be optically resolved, while luminescence was discernible for samples with a pitch size larger than 600 nm (Figure 3c).

The UCNPs embedded in lateral gap-mode cavities with a high local density of states can probe a large pumping photon flux. The effective area for generating luminescence signals is the nanotrench region where the nanoparticles are trapped. To quantify the enhancement factors (EFs) for UCNPs coupled to plasmonic nanotrenches, emission intensities were normalized by effective area correction using the following formula (Figure 3c and Figure S9)

$$\langle \mathrm{EF} \rangle = \frac{I_{\mathrm{gap}}}{I_{\mathrm{glass/gold}}} \times \frac{A_{\mathrm{spot}}}{A_{\mathrm{gap}}} \quad (1)$$

where I_{gap} is the luminescence intensity measured for UCNPs localized within nanotrenches, I_{gold} and I_{glass} are emission intensities measured for a monolayer of UCNPs deposited on a gold film or glass slide (Figure S8), and A_{gap} is the effective area of plasmonic nanotrenches (see SI).

The enhancement factor dependence of green and red emissions on different pitch sizes is summarized in Figure 3d. The maximum green emission intensity of UCNPs coupled to gold nanostructures is about 500 and 370 times higher than that of UCNPs deposited on an unpatterned gold film and glass slide, respectively, while the red emission intensity is enhanced by more than 7000- and 2000-fold (Table S1 and S2). We next performed power-dependent investigations of emission at 540 and 655 nm for UCNPs coupled to the nanocavity and two control substrates (Figure S10). Luminescence spectra with small deviations were collected from three random areas on each sample. We plotted the upconversion emission intensity as a function of the power density on a double-logarithmic scale (Figure 3e,g). Under weak excitation, the slopes of the green and red emission for samples deposited on the glass substrate were 1.31 and 1.53, respectively, while increasing to 1.34 and 1.85 on the flat gold substrate. For both control samples, the red emission features a larger slope than the green emission, suggesting a higher-order photon population process for the former. In contrast, for UCNPs located in plasmonic nanotrenches, the slopes of green and red emissions were reduced to 0.71 and 0.94, respectively, indicating early onset of pump saturation due to optical field enhancement at the absorption band. The power dependence on the emission enhancement factor also revealed that the effect of pump fluence on emission intensity under low-power excitation is more significant than under high-power excitation. Compared with samples on a glass substrate, green and red emissions were enhanced by a factor of 1600 and 10 000, respectively, at low pumping power for nanocavity-coupled UCNPs. Conversely, nanocavity-coupled UCNPs showed enhancement factors of up to 2000 and 20 000 for green and red emissions, respectively, relative to samples on the gold substrate (Figure 3f and Figure S11).

It is important to note that a good match between the fundamental mode of the coupled UCNP−gold nanostructure and the wavelength of the pumping laser can amplify the excitation rate of UCNPs, while mode-matching of the plasmon resonance and the emission wavelength of UCNPs is likely to increase the radiative decay rate via the Purcell effect.[33] We attained higher EFs when the plasmon resonance was located spectrally closer to the excitation than the emission band of UCNPs. This result suggests that the excitation enhancement dominates the global luminescence enhancement, while the decay rate enhancement is a less prominent factor.

It is also interesting to note that the red emission intensity was systematically more enhanced than the green one. The enhancement is strongly influenced by the number of photons involved in upconversion. Multiphoton paths exhibit higher power sensitivity than linear optical processes.[35,49,50] In the lanthanide-mediated upconversion, long-lived intermediate excited states serve as energy reservoirs that sequentially populate higher emitting energy levels. The dependence of emission intensity, I, on excitation power density, P_{exc}, can be

https://dx.doi.org/10.1021/acs.nanolett.1c00232
Nano Lett. 2021, 21, 3044−3051

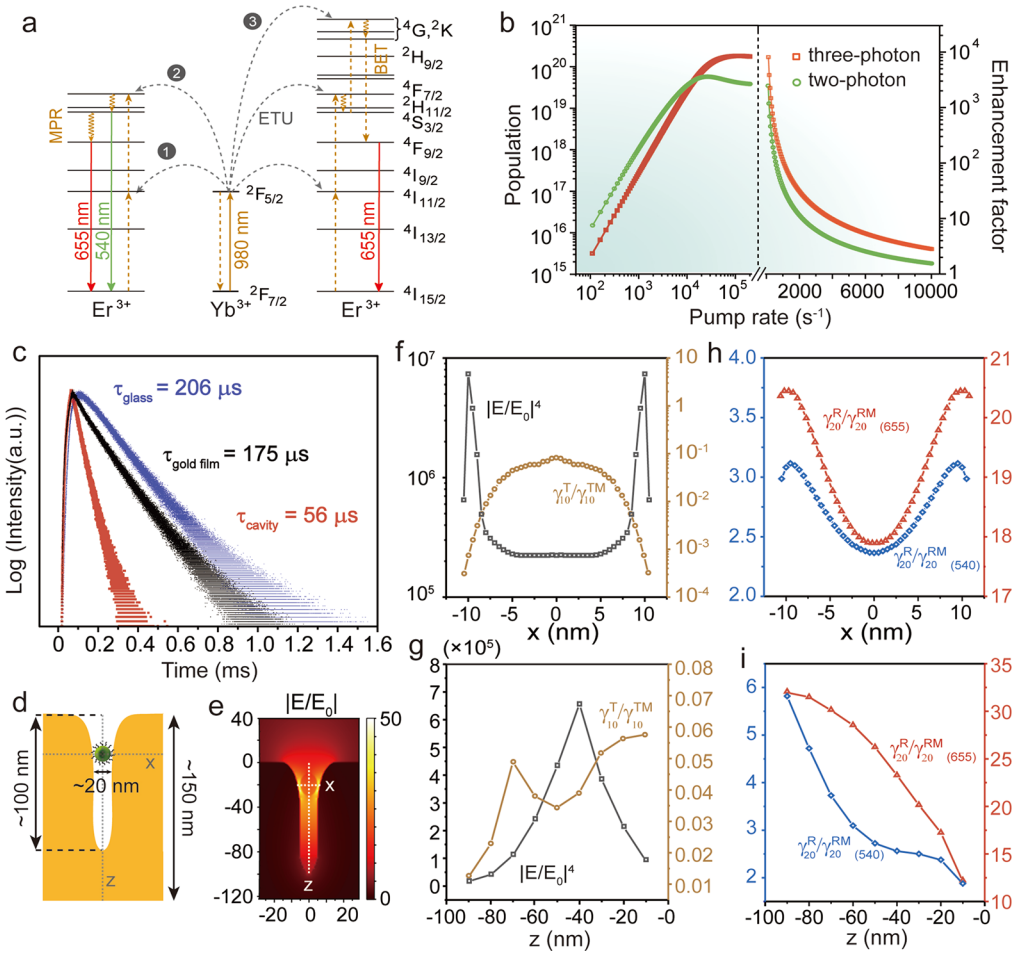

Figure 4. Theoretical investigations of the gap-plasmon upconversion acceleration. (a) Energy level diagram of $NaYF_4$:Yb/Er nanoparticles and proposed excitation paths for green (~540 nm) and red (~655 nm) emission under 980 nm excitation. The green emitting state ($^4S_{3/2}$) of Er^{3+} is first populated via two successive energy transfer upconversion (ETU) steps ($^4I_{15/2} \rightarrow {}^4I_{11/2}$, $^4I_{11/2} \rightarrow {}^4F_{7/2}$) from neighboring Yb^{3+} ions in the host, followed by nonradiative multiphonon relaxation (MPR) of Er^{3+} ($^4F_{7/2} \rightarrow {}^4S_{3/2}$). The red-emitting state, $^4F_{9/2}$, is subsequently populated via MPR from the green-emitting state in the two-photon process. In the three-photon process, a third ETU step promotes the photon further to the dense manifold of states (^4G, ^2K). Then a back-energy-transfer (BET) process from Er^{3+} to ground-level Yb^{3+} can also yield red emission. (b) Numerical simulations of power dependence (left) and enhancement factors (right) based on a simplified energy transfer model involving two- and three-photon upconversion processes. (c) Emission lifetime measurements at 655 nm for UCNPs embedded in plasmonic nanotrenches (yellow) and deposited on a glass slide (blue) or gold film (black). (d,e) Schematic and cross-sectional electric-field distributions of the UCNP-coupled gap nanocavity (*xz* plane). The depth and width of the gap are slightly modified to keep the resonant wavelength close to 980 nm. (f,g) The fourth power of local E-field-induced absorption enhancement factors (black) and relaxation factor (brown) as a function of *x*-position and *z*-position within the gap. (h,i) Normalized radiative decay rates at 540 nm (blue) and 655 nm (red) for a dipole emitter located at different *x*-position and *z*-position within the gap. Decay rates are averaged by inserting a dipole in three orthogonal directions.

expressed as $I \propto P^n_{exc}$ in the weak excitation limit, where n is the number of upconversion steps involved.[50] In our study, Yb^{3+}/Er^{3+} codoped UCNPs emit two peaks at 540 nm (green) and 655 nm (red) under 980 nm excitation. The green emission mainly results from two-photon excitation, while both two-photon and three-photon processes are mainly responsible for red upconversion emission (Figure 4a).[51,52] To investigate the pump power sensitivity of the multiphoton upconversion in Yb^{3+}/Er^{3+} codoped UCNPs, a population kinetic model involving two- and three-photon populations was numerically constructed (Figure 4b, Figure S12, and Table S3). Simulation results show that multiphoton paths exhibit higher excitation power sensitivity, confirming that significant luminescence enhancement of UCNPs likely occurs in plasmonic mode-mediated, higher-order photon population.

The increased local density of states within plasmon nanotrenches may lead to changes in the excited-state lifetime of emitters. The temporal decay investigation showed that UCNPs on the glass slide exhibit monoexponential decay with a decay lifetime of 206 μs at 655 nm, whereas UCNPs on the gold film have a decay lifetime of 175 μs (Figure 4c). This slight reduction in the lifetime was attributed to surface quenching due to nonradiative energy transfer between UCNPs and the gold film. Intriguingly, when UCNPs were self-assembled in the plasmonic nanotrench, their luminescence lifetime drastically shortened to 56 μs, corresponding to a 3.7-fold increase in the upconversion emission rate. In this case, except for the quenching effect, we reason that the shortened lifetime is primarily attributed to increased radiative decay due to the Purcell effect.

To further probe the mechanism underlying luminescence enhancement, an excited-state absorption (ESA)-mediated upconversion process in a plasmonic nanocavity was numerically investigated based on a 3D-FDTD (finite difference time

https://dx.doi.org/10.1021/acs.nanolett.1c00232
Nano Lett. 2021, 21, 3044−3051

domain) method (Figure S13).[53] The nanopatterned substrate with an optimized pitch size of 300 nm was chosen, and the incident light was simulated as an *x*-polarized plane wave at 980 nm (Figure 4d,e). For ESA-mediated upconversion, two competing processes contribute to plasmon-induced excitation enhancement: the ground-state absorption improvement arising from the fourth power of near-field enhancement and the relaxation factor due to spontaneous transition from the intermediate state to the ground state. Simulated position-dependent results show significant absorption enhancement with a maximum factor exceeding 10^6 near the corner of the nanogap (Figure 4f,g), indicating an extremely confined gap-plasmon mode with a large local density of sates. The corresponding decay rate enhancements as a function of emitter positions located along *x*- and *z*-axes revealed a plasmon-induced emission acceleration with maximum decay rate enhancement factors of more than 40 and 10 for red and green emission, respectively (Figure 4h,i). These numerical simulations suggest that the excitation enhancement dominates the nonlinear upconversion, and the enhanced luminescence is accompanied by increased emission decay rate, which agrees well with experimental results.

In summary, we demonstrated strong light−matter coupling by placing UCNPs into nanometric photonic hotspots of gold nanotrenches. This integrated nanoscale platform strongly confined incident excitation radiation within deep subwavelength metallic nanogaps, leading to 10 000-fold and 3.7-fold enhancement in luminescence intensity and emission rate, respectively. The ability to engineer optical density of states in subwavelength metallic nanotrenches on-demand provides sufficient optical tunability of population kinetics for nonlinear light generation. Our lateral gap-mode platform for multiphoton upconversion amplification can even be extended to other types of nonlinear processes such as triplet−triplet annihilation, multiple harmonic generation, and multiphoton absorption. These results lay the foundation for the design of state-of-the-art gap-mode nanocavities for frequency conversion enhancement while providing new perspectives for the realization of high-sensitivity biosensors, bright and fast quantum light sources, and low-threshold upconverted nanolasers.

■ ASSOCIATED CONTENT

Supporting Information

The Supporting Information is available free of charge at https://pubs.acs.org/doi/10.1021/acs.nanolett.1c00232.

Nanocrystal synthesis, fabrication process of template-stripped gold substrates, nanoparticle assembly, calculation for upconversion enhancement factors by area correction, numerical simulations, 3D-FDTD simulation conditions, AFM measurements, TEM image and XRD pattern of nanoparticles, optical reflectance spectra of gold film, SEM images of assembled UCNPs, power-dependent upconversion photoluminescence, energy diagram and kinetic parameters for the sensitizer-activator upconversion system, ESA-mediated upconversion process (PDF)

■ AUTHOR INFORMATION

Corresponding Authors

Xiaogang Liu − *Department of Chemistry and The N.1 Institute for Health, National University of Singapore, Singapore 117543, Singapore; Joint School of National University of Singapore and Tianjin, University International Campus of Tianjin University, Fuzhou 350207, P.R. China;* orcid.org/0000-0003-2517-5790; Email: chmlx@nus.edu.sg

Joel K. W. Yang − *Institute of Materials Research and Engineering, A*STAR (Agency for Science, Technology and Research), Singapore 138634, Singapore; Singapore University of Technology and Design, Singapore 487372, Singapore;* orcid.org/0000-0003-3301-1040; Email: joel_yang@sutd.edu.sg

Authors

Jiahui Xu − *Department of Chemistry and The N.1 Institute for Health, National University of Singapore, Singapore 117543, Singapore*

Zhaogang Dong − *Institute of Materials Research and Engineering, A*STAR (Agency for Science, Technology and Research), Singapore 138634, Singapore;* orcid.org/0000-0002-0929-7723

Mohamed Asbahi − *Institute of Materials Research and Engineering, A*STAR (Agency for Science, Technology and Research), Singapore 138634, Singapore*

Yiming Wu − *Department of Chemistry and The N.1 Institute for Health, National University of Singapore, Singapore 117543, Singapore*

Hao Wang − *Singapore University of Technology and Design, Singapore 487372, Singapore*

Liangliang Liang − *Department of Chemistry and The N.1 Institute for Health, National University of Singapore, Singapore 117543, Singapore;* orcid.org/0000-0003-4958-3801

Ray Jia Hong Ng − *Singapore University of Technology and Design, Singapore 487372, Singapore*

Hailong Liu − *Singapore University of Technology and Design, Singapore 487372, Singapore*

Renaud A. L. Vallée − *CNRS, University of Bordeaux, Pessac 33600, France*

Complete contact information is available at: https://pubs.acs.org/10.1021/acs.nanolett.1c00232

Notes

The authors declare no competing financial interest.

■ ACKNOWLEDGMENTS

This work is supported by the National Key & Program of China (No. 2018YFA0902600), the National Natural Science Foundation of China (21635002, 21771135, 21871071), the Ministry of Education, Singapore (MOE2017-T2-2-110), the Agency for Science, Technology and Research (A*STAR) (Grant A1883c0011, A1983c0038, A20E5c0093), A*STAR SERC Pharos Project (Grant 1527300025), and National Research Foundation, the Prime Minister's Office of Singapore under its NRF Investigatorship Programme (Award No. NRF-NRFI05-2019-0003). Z.D. acknowledges the funding support by A*STAR career development award (CDA). We also thank P. Lu, Z. Mu, and D. Ding for technical assistance and helpful discussion.

■ REFERENCES

(1) Cai, W.; Vasudev, A. P.; Brongersma, M. L. Electrically Controlled Nonlinear Generation of Light with Plasmonics. *Science* **2011**, *333*, 1720−1723.

(2) Wang, Z.; Dong, Z.; Gu, Y.; Chang, Y. H.; Zhang, L.; Li, L. J.; Zhao, W.; Eda, G.; Zhang, W.; Grinblat, G.; Maier, S. A.; Yang, J. K. W.; Qiu, C. W.; Wee, A. T. S. Giant Photoluminescence Enhancement in Tungsten-Diselenide-Gold Plasmonic Hybrid Structures. *Nat. Commun.* **2016**, *7*, 11283.
(3) Luo, Y.; Shepard, G. D.; Ardelean, J. V.; Rhodes, D. A.; Kim, B.; Barmak, K.; Hone, J. C.; Strauf, S. Deterministic Coupling of Site-Controlled Quantum Emitters in Monolayer WSe_2 to Plasmonic Nanocavities. *Nat. Nanotechnol.* **2018**, *13*, 1137−1142.
(4) Fernandez-Bravo, A.; Wang, D.; Barnard, E. S.; Teitelboim, A.; Tajon, C.; Guan, J.; Schatz, G. C.; Cohen, B. E.; Chan, E. M.; Schuck, P. J.; Odom, T. W. Ultralow-Threshold, Continuous-Wave Upconverting Lasing from Subwavelength Plasmons. *Nat. Mater.* **2019**, *18*, 1172−1176.
(5) Seyler, K. L.; Schaibley, J. R.; Gong, P.; Rivera, P.; Jones, A. M.; Wu, S.; Yan, J.; Mandrus, D. G.; Yao, W.; Xu, X. Electrical Control of Second-Harmonic Generation in a WSe_2 Monolayer Transistor. *Nat. Nanotechnol.* **2015**, *10*, 407−411.
(6) Das, A.; Mao, C.; Cho, S.; Kim, K.; Park, W. Over 1000-Fold Enhancement of Upconversion Luminescence Using Water-Dispersible Metal-Insulator-Metal Nanostructures. *Nat. Commun.* **2018**, *9*, 4828.
(7) Celebrano, M.; Wu, X.; Baselli, M.; Großmann, S.; Biagioni, P.; Locatelli, A.; De Angelis, C.; Cerullo, G.; Osellame, R.; Hecht, B.; Duò, L.; Ciccacci, F.; Finazzi, M. Mode Matching in Multiresonant Plasmonic Nanoantennas for Enhanced Second Harmonic Generation. *Nat. Nanotechnol.* **2015**, *10*, 412−417.
(8) Dong, Z.; Asbahi, M.; Lin, J.; Zhu, D.; Wang, Y. M.; Hippalgaonkar, K.; Chu, H. S.; Goh, W. P.; Wang, F.; Huang, Z.; Yang, J. K. W. Second-Harmonic Generation from Sub-5 nm Gaps by Directed Self-Assembly of Nanoparticles onto Template-Stripped Gold Substrates. *Nano Lett.* **2015**, *15*, 5976−5981.
(9) Aouani, H.; Rahmani, M.; Navarro-Cía, M.; Maier, S. A. Third-Harmonic-Upconversion Enhancement from a Single Semiconductor Nanoparticle Coupled to a Plasmonic Antenna. *Nat. Nanotechnol.* **2014**, *9*, 290−294.
(10) Fan, Y.; Wang, P.; Lu, Y.; Wang, R.; Zhou, L.; Zheng, X.; Li, X.; Piper, J. A.; Zhang, F. Lifetime-Engineered NIR-II Nanoparticles Unlock Multiplexed in Vivo Imaging. *Nat. Nanotechnol.* **2018**, *13*, 941−946.
(11) Gai, S.; Li, C.; Yang, P.; Lin, J. Recent Progress in Rare Earth Micro/Nanocrystals: Soft Chemical Synthesis, Luminescent Properties, and Biomedical Applications. *Chem. Rev.* **2014**, *114*, 2343−2389.
(12) Liang, L.; Qin, X.; Zheng, K.; Liu, X. Energy Flux Manipulation in Upconversion Nanosystems. *Acc. Chem. Res.* **2019**, *52*, 228−236.
(13) Nadort, A.; Zhao, J.; Goldys, E. M. Lanthanide Upconversion Luminescence at the Nanoscale: Fundamentals and Optical Properties. *Nanoscale* **2016**, *8*, 13099−13130.
(14) Haase, M.; Schäfer, H. Upconverting Nanoparticles. *Angew. Chem., Int. Ed.* **2011**, *50*, 5808−5829.
(15) Liu, Y.; Meng, X.; Bu, W. Upconversion-Based Photodynamic Cancer Therapy. *Coord. Chem. Rev.* **2019**, *379*, 82−98.
(16) Marin, R.; Labrador-Paéz, L.; Skripka, A.; Haro-González, P.; Benayas, A.; Canton, P.; Jaque, D.; Vetrone, F. Upconverting Nanoparticle to Quantum Dot Förster Resonance Energy Transfer: Increasing the Efficiency through Donor Design. *ACS Photonics* **2018**, *5*, 2261−2270.
(17) Liu, Y.; Lu, Y.; Yang, X.; Zheng, X.; Wen, S.; Wang, F.; Vidal, X.; Zhao, J.; Liu, D.; Zhou, Z.; Ma, C.; Zhou, J.; Piper, J. A.; Xi, P.; Jin, D. Amplified Stimulated Emission in Upconversion Nanoparticles for Super-Resolution Nanoscopy. *Nature* **2017**, *543*, 229−233.
(18) Zheng, W.; Huang, P.; Tu, D.; Ma, E.; Zhu, H.; Chen, X. Lanthanide-Doped Upconversion Nano-Bioprobes: Electronic Structures, Optical Properties, and Biodetection. *Chem. Soc. Rev.* **2015**, *44*, 1379−1415.
(19) Huang, L.; Zhao, Y.; Zhang, H.; Huang, K.; Yang, J.; Han, G. Expanding Anti-Stokes Shifting in Triplet-Triplet Annihilation Upconversion for In Vivo Anticancer Prodrug Activation. *Angew. Chem.* **2017**, *129*, 14592−14596.
(20) Tan, M.; Tan, M.; Tan, M.; Li, F.; Li, F.; Li, F.; Wang, X.; Fan, R.; Chen, G.; Chen, G.; Chen, G. Temporal Multilevel Luminescence Anticounterfeiting through Scattering Media. *ACS Nano* **2020**, *14*, 6532−6538.
(21) Qin, X.; Xu, J.; Wu, Y.; Liu, X. Energy-Transfer Editing in Lanthanide-Activated Upconversion Nanocrystals: A Toolbox for Emerging Applications. *ACS Cent. Sci.* **2019**, *5*, 29−42.
(22) Dong, H.; Sun, L. D.; Feng, W.; Gu, Y.; Li, F.; Yan, C. H. Versatile Spectral and Lifetime Multiplexing Nanoplatform with Excitation Orthogonalized Upconversion Luminescence. *ACS Nano* **2017**, *11*, 3289−3297.
(23) Wen, S.; Zhou, J.; Zheng, K.; Bednarkiewicz, A.; Liu, X.; Jin, D. Advances in Highly Doped Upconversion Nanoparticles. *Nat. Commun.* **2018**, *9*, 2415.
(24) Kim, S. Y.; Woo, K.; Lim, K.; Lee, K.; Jang, H. S. Highly Bright Multicolor Tunable Ultrasmall β-Na(Y,Gd)F_4:Ce,Tb,Eu/β-$NaYF_4$ Core/Shell Nanocrystals. *Nanoscale* **2013**, *5*, 9255−9263.
(25) Zhang, W.; Ding, F.; Chou, S. Y. Large Enhancement of Upconversion Luminescence of $NaYF_4$:Yb^{3+}/Er^{3+} Nanocrystal by 3D Plasmonic Nano-Antennas. *Adv. Mater.* **2012**, *24*, OP236−OP241.
(26) Liu, H.; Xu, J.; Wang, H.; Liu, Y.; Ruan, Q.; Wu, Y.; Liu, X.; Yang, J. K. W. Tunable Resonator-Upconverted Emission (TRUE) Color Printing and Applications in Optical Security. *Adv. Mater.* **2019**, *31*, 1807900.
(27) Lee, G. Y.; Jung, K.; Jang, H. S.; Kyhm, J.; Han, I. K.; Park, B.; Ju, H.; Kwon, S. J.; Ko, H. Upconversion Luminescence Enhancement in Plasmonic Architecture with Random Assembly of Metal Nanodomes. *Nanoscale* **2016**, *8*, 2071−2080.
(28) Park, W.; Lu, D.; Ahn, S. Plasmon Enhancement of Luminescence Upconversion. *Chem. Soc. Rev.* **2015**, *44*, 2940−2962.
(29) Debasu, M. L.; Ananias, D.; Pastoriza-Santos, I.; Liz-Marzán, L. M.; Rocha, J.; Carlos, L. D. All-in-One Optical Heater-Thermometer Nanoplatform Operative from 300 to 2000 K Based on Er^{3+} Emission and Blackbody Radiation. *Adv. Mater.* **2013**, *25*, 4868−4874.
(30) Bang, D.; Jo, E. J.; Hong, S.; Byun, J. Y.; Lee, J. Y.; Kim, M. G.; Lee, L. P. Asymmetric Nanocrescent Antenna on Upconversion Nanocrystal. *Nano Lett.* **2017**, *17*, 6583−6590.
(31) Wang, T.; Siu, C. K.; Yu, H.; Wang, Y.; Li, S.; Lu, W.; Hao, J.; Liu, H.; Teng, J. H.; Lei, D. Y.; Xu, X.; Yu, S. F. Influence of Plasmonic Effect on the Upconversion Emission Characteristics of $NaYF_4$ Hexagonal Microrods. *Inorg. Chem.* **2018**, *57*, 8200−8204.
(32) Gong, C.; Liu, W.; He, N.; Dong, H.; Jin, Y.; He, S. Upconversion Enhancement by a Dual-Resonance All-Dielectric Metasurface. *Nanoscale* **2019**, *11*, 1856−1862.
(33) Lu, D.; Cho, S. K.; Ahn, S.; Brun, L.; Summers, C. J.; Park, W. Plasmon Enhancement Mechanism for the Upconversion Processes in $NaYF_4$:Yb^{3+},Er^{3+} Nanoparticles: Maxwell versus Förster. *ACS Nano* **2014**, *8*, 7780−7792.
(34) Zhou, D.; Liu, D.; Xu, W.; Yin, Z.; Chen, X.; Zhou, P.; Cui, S.; Chen, Z.; Song, H. Observation of Considerable Upconversion Enhancement Induced by $Cu_{2-X}S$ Plasmon Nanoparticles. *ACS Nano* **2016**, *10*, 5169−5179.
(35) Chen, B.; Liu, Y.; Xiao, Y.; Chen, X.; Li, Y.; Li, M.; Qiao, X.; Fan, X.; Wang, F. Amplifying Excitation-Power Sensitivity of Photon Upconversion in a $NaYbF_4$:Ho Nanostructure for Direct Visualization of Electromagnetic Hotspots. *J. Phys. Chem. Lett.* **2016**, *7*, 4916−4921.
(36) Wu, Y.; Xu, J.; Liu, X. Controlled Patterning of Upconversion Nanocrystals through Capillary Force. *J. Rare Earths* **2020**, *38*, 546−551.
(37) Siegfried, T.; Ekinci, Y.; Martin, O. J. F.; Sigg, H. Gap Plasmons and Near-Field Enhancement in Closely Packed Sub-10 nm Gap Resonators. *Nano Lett.* **2013**, *13*, 5449−5453.
(38) Park, K. D.; Jiang, T.; Clark, G.; Xu, X.; Raschke, M. B. Radiative Control of Dark Excitons at Room Temperature by Nano-Optical Antenna-Tip Purcell Effect. *Nat. Nanotechnol.* **2018**, *13*, 59−64.
(39) Wu, Y.; Xu, J.; Poh, E. T.; Liang, L.; Liu, H.; Yang, J. K. W.; Qiu, C. W.; Vallée, R. A. L.; Liu, X. Upconversion Superburst with Sub-2 μs Lifetime. *Nat. Nanotechnol.* **2019**, *14*, 1110−1115.

https://dx.doi.org/10.1021/acs.nanolett.1c00232
Nano Lett. 2021, 21, 3044−3051

(40) Groß, H.; Hamm, J. M.; Tufarelli, T.; Hess, O.; Hecht, B. Near-Field Strong Coupling of Single Quantum Dots. *Sci. Adv.* **2018**, *4*, No. eaar4906.
(41) Ojambati, O. S.; Chikkaraddy, R.; Deacon, W. M.; Huang, J.; Wright, D.; Baumberg, J. J. Efficient Generation of Two-Photon Excited Phosphorescence from Molecules in Plasmonic Nanocavities. *Nano Lett.* **2020**, *20*, 4653−4658.
(42) Kim, M.; Ko, S. M.; Kim, J. M.; Son, J.; Lee, C.; Rhim, W. K.; Nam, J. M. Dealloyed Intra-Nanogap Particles with Highly Robust, Quantifiable Surface-Enhanced Raman Scattering Signals for Biosensing and Bioimaging Applications. *ACS Cent. Sci.* **2018**, *4*, 277−287.
(43) Nam, J. M.; Oh, J. W.; Lee, H.; Suh, Y. D. Plasmonic Nanogap-Enhanced Raman Scattering with Nanoparticles. *Acc. Chem. Res.* **2016**, *49*, 2746−2755.
(44) Nagpal, P.; Lindquist, N. C.; Oh, S. H.; Norris, D. J. Ultrasmooth Patterned Metals for Plasmonics and Metamaterials. *Science* **2009**, *325*, 594−597.
(45) Asbahi, M.; Wang, F. K.; Dong, Z. G.; Yang, J. K. W.; Chong, K. S. L. Directed self-assembly of sub-10nm particle clusters using topographical templates. *Nanotechnology* **2016**, *27*, 424001.
(46) Gargas, D. J.; Chan, E. M.; Ostrowski, A. D.; Aloni, S.; Altoe, M. V. P.; Barnard, E. S.; Sanii, B.; Urban, J. J.; Milliron, D. J.; Cohen, B. E.; Schuck, P. J. Engineering Bright Sub-10-nm Upconverting Nanocrystals for Single-Molecule Imaging. *Nat. Nanotechnol.* **2014**, *9*, 300−305.
(47) Liu, Q.; Zhang, Y.; Peng, C. S.; Yang, T.; Joubert, L. M.; Chu, S. Single Upconversion Nanoparticle Imaging at Sub-10 W cm^{-2} Irradiance. *Nat. Photonics* **2018**, *12*, 548−553.
(48) Saboktakin, M.; Ye, X.; Chettiar, U. K.; Engheta, N.; Murray, C. B.; Kagan, C. R. Plasmonic Enhancement of Nanophosphor Upconversion Luminescence in Au Nanohole Arrays. *ACS Nano* **2013**, *7*, 7186−7192.
(49) Liang, L.; Teh, D. B. L.; Dinh, N. D.; Chen, W.; Chen, Q.; Wu, Y.; Chowdhury, S.; Yamanaka, A.; Sum, T. C.; Chen, C. H.; Thakor, N. V.; All, A. H.; Liu, X. Upconversion Amplification through Dielectric Superlensing Modulation. *Nat. Commun.* **2019**, *10*, 1391.
(50) Suyver, J. F.; Aebischer, A.; García-Revilla, S.; Gerner, P.; Güdel, H. U. Anomalous Power Dependence of Sensitized Upconversion Luminescence. *Phys. Rev. B - Condens. Matter Mater. Phys.* **2005**, *71*, 1098.
(51) Berry, M. T.; May, P. S. Disputed Mechanism for NIR-to-Red Upconversion Luminescence in $NaYF_4$:Yb^{3+},Er^{3+}. *J. Phys. Chem. A* **2015**, *119*, 9805−9811.
(52) Hossan, M. Y.; Hor, A.; Luu, Q.; Smith, S. J.; May, P. S.; Berry, M. T. Explaining the Nanoscale Effect in the Upconversion Dynamics of β-$NaYF_4$:Yb^{3+}, Er^{3+} Core and Core-Shell Nanocrystals. *J. Phys. Chem. C* **2017**, *121*, 16592−16606.
(53) Liu, X.; Lei, D. Y. Simultaneous Excitation and Emission Enhancements in Upconversion Luminescence Using Plasmonic Double-Resonant Gold Nanorods. *Sci. Rep.* **2015**, *5*, 15235.

https://dx.doi.org/10.1021/acs.nanolett.1c00232
Nano Lett. 2021, 21, 3044−3051